Transmission electron microscopy

Franken, Linda Elise

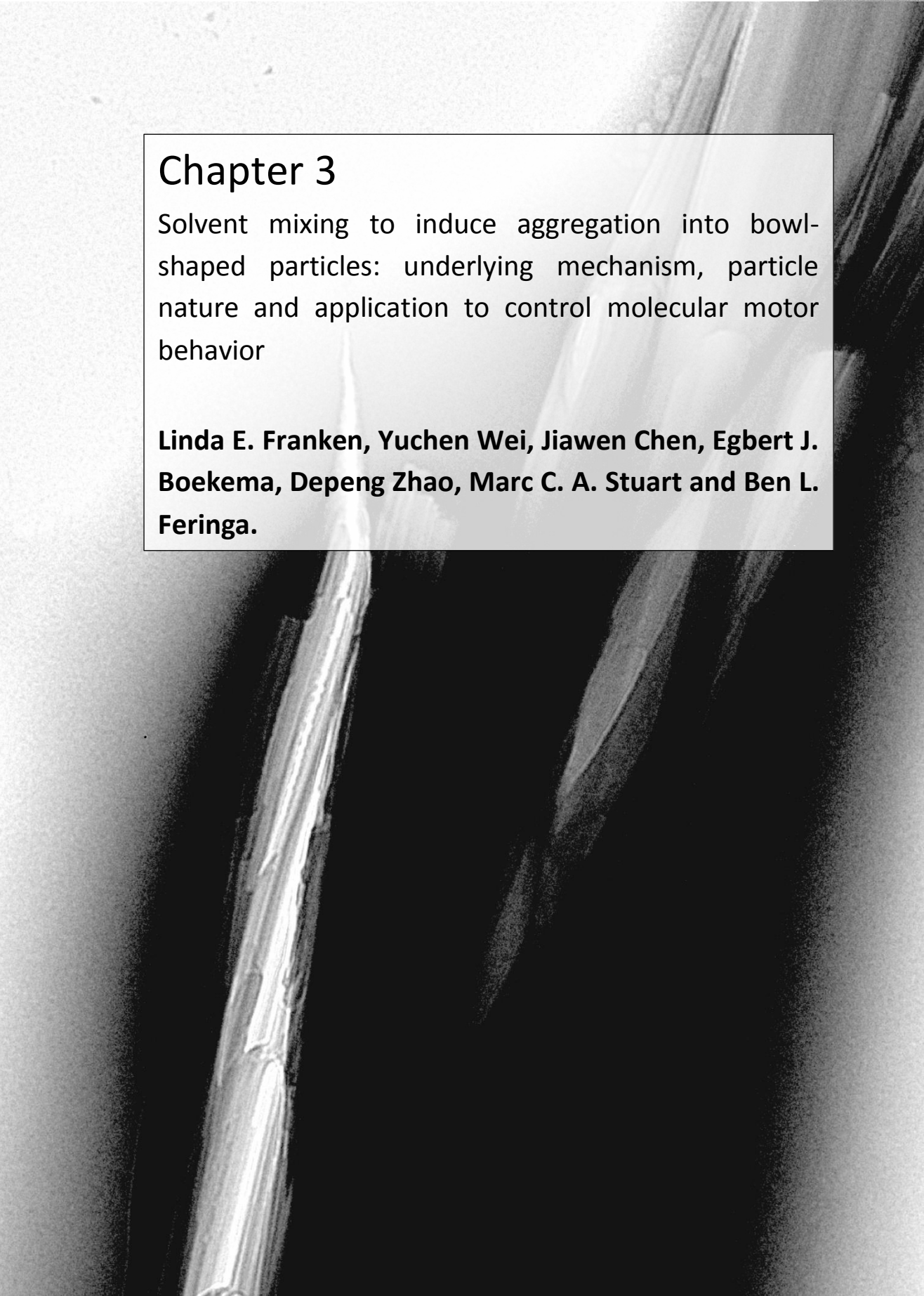

Chapter 3

Solvent mixing to induce aggregation into bowl-shaped particles: underlying mechanism, particle nature and application to control molecular motor behavior

Linda E. Franken, Yuchen Wei, Jiawen Chen, Egbert J. Boekema, Depeng Zhao, Marc C. A. Stuart and Ben L. Feringa.

Abstract

The mixing of a good solvent and a (partial) non-solvent to induce aggregation to transfer amphiphilic or even hydrophobic molecules into for example an aqueous environment is common practice. With strong amphiphiles, this transfer process can induce self-assembly of molecules into micelles, vesicles and other morphologies. Here we provide evidence that in the case of bowl-shaped aggregates the structures are not the product of self-assembly, but a direct result of the solvent mixing. With examples from literature as well as various hydrophobic molecules we demonstrate that the process is nonspecific and highly independent of the molecular design. Under influence of the non-solvent, droplets are formed, of which the exterior is hardened due to the increased glass-transition temperature by the external medium, while the interior of the droplets remains plasticized by the solvent. The shrinking exterior versus plasticized interior results in the formation of extremely stable glass-like nano-droplets with a fluid interior, a glass-like exterior and a very specific shape: dense spheres with a hole in their side. Depending on the amount of solvent versus non-solvent, the aggregate size and thus the confinement can be reversibly controlled. Applying this to a bulky first generation molecular motor allowed us to change its isomerization behavior. Strong confinement prohibits the thermal helix inversion step while altering the energy barriers that determine the rotary motion such that it introduces a reverse trans-cis isomerization by heating. Furthermore the motor shows in situ photo-switchable aggregation-induced emission (AIE).

Keywords: solvent selectivity, molecular reorganization, TEM, self-assembly, molecular motor

Author contributions: Literature observations: MCAS and LEF; Concept, supervision and design: B.F and MCAS; Synthesis of molecular motor 1: YW, DZ and JC; Aggregate characterizations: LEF, YW and MCAS; Mechanism: LEF and MCAS; Fluorescence: YW and MCAS; Manuscript writing: LEF, YW and MCAS. All authors have contributed and given approval to the final version of the manuscript.

1. Introduction

The development and functionalization of molecules that can assemble into larger structures such as gels or vesicles has undergone rapid advance in recent years (Decher, 1997; Zeng and Zimmerman, 1997; Grzelczak *et al.*, 2010; Allen and Cullis, 2013). These advances are illustrated by the development of new functionalized materials such as responsive materials (Ganta *et al.*, 2008; Stuart *et al.*, 2010; Jochum and Theato, 2013; Mura *et al.*, 2013), self-healing materials (Schneider *et al.*, 2002; Toohey *et al.*, 2007; Cordier *et al.*, 2008; Zhang *et al.*, 2012) and loaded nano-carriers (Yokoyama *et al.*, 1998; Torchilin, 2007; Yang *et al.*, 2010a; Nicolas *et al.*, 2013). Many different structures are being made with increasing control over properties such as morphology (Park *et al.*, 2003; Groeschel *et al.*, 2012; Mai and Eisenberg, 2012), (dis-) assembly (Hartgerink *et al.*, 2002), rheology (Tzoganakis *et al.*, 1988; Berzin *et al.*, 2001), orthogonality (Brizard *et al.*, 2008) and size (Denisov *et al.*, 2004).

One particular morphology has drawn our attention as it is both very specific in its shape and very general in its occurrence. Its morphology comprises a dense, spherical aggregate which often has one and occasionally more dents in its surface. This morphology has been termed by various names including hollow spheres (Im *et al.*, 2005; Yang *et al.*, 2010b; Maity *et al.*, 2011), dimple-like aggregate (Liu *et al.*, 2009), dimpled beads (Wang *et al.*, 2004), cup-like aggregate (Li *et al.*, 2014) and bowl-shape (Riegel *et al.*, 2002; Riegel *et al.*, 2004; Yang *et al.*, 2010b). Although these terms seem to describe only the shape and not the nature of the morphologies, we avoid introducing yet another name and follow the term bowl-shape. More worriedly, this structure has also been mistakenly identified as (large compound) micelle (Jin *et al.*, 2012; Sun and Liu, 2012; Yao *et al.*, 2014; Jiang *et al.*, 2014) or vesicle (polymersome). The peculiar dent makes that the structure is easily mistaken for a (collapsed) vesicle. When only scanning electron microscopy (SEM) is used without transmission electron microscopy (TEM), the two morphologies cannot even be separated as demonstrated by the figures from Yang *et al.* (2010b).

Even though this morphology is equally specific as a double membrane-layer would be, it is found in connection with a very wide range of molecules: amphiphiles (Riegel *et al.*, 2002; Mitra *et al.*, 2013; He *et al.*, 2015), pseudo-amphiphiles (Alfonso *et al.*, 2010), hydrophobic molecules (Im *et al.*, 2005; Jin *et al.*, 2012), block copolymers and many others (Wang *et al.*, 2004; Liu *et al.*,

2009; Jiang *et al.*, 2014). Yet the general principle behind the formation of these bowl-shaped aggregates, the general applicability of the method and the understanding of the morphology are to our knowledge not yet elucidated. Here we use non-amphiphilic molecules to demonstrate that the morphology can be created without the influence of molecular design, unambiguously disputing self-assembly (Whitesides and Grzybowski, 2002) and the possibility of a micellar or vesicular nature. Furthermore, our cryo-TEM images undeniably contradict a hollow nature.

Careful inspection of the methods that were used to obtain these structures leads to the observation that only two methods were used. One is the evaporation of solvents. The other is the most commonly used and the focus of this work: the induction of aggregation by the mixing of solvents (Riegel *et al.*, 2002; Vriezema *et al.*, 2003; Riegel *et al.*, 2004; Wang *et al.*, 2004; Vriezema *et al.*, 2007; van Dongen *et al.*, 2009; Li *et al.*, 2014; Yao *et al.*, 2014; Jiang *et al.*, 2014; He *et al.*, 2015). Tuning self-assembly of several amphiphilic block copolymers into various morphologies by selective solvent mixtures has been successfully shown by, for example, Eisenberg *et al.*. However, in the case of the bowl-shaped morphology, it can be argued that the driving force of solvent mixing cannot be called self-assembly, because the molecular design of the components does not control assembly (Whitesides and Grzybowski, 2002). Instead, the reorganization is completely solvent driven. Although applications of the structures have already been envisioned and some even tested, the lack of understanding of the morphology and nature of the particles currently hinders exploration and design of applications.

The promising research field of aggregation induced emission (AIE) describes a class of molecules that become fluorescently active upon aggregation and have great potential for sensing, imaging and optoelectronic applications (Luo *et al.*, 2001; Wang *et al.*, 2012; Mei *et al.*, 2014; Mei *et al.*, 2015; Zhao *et al.*, 2015b; Liu, 2016). In order to explore the potential for application of the bowl-shaped morphologies, we use solvent mixing to study a novel molecular motor **1** (Figure 3-1). The bulky fluorophore-like groups are predicted to exhibit photo-active behavior while the motor is an overcrowded alkene-based molecular motor. It belongs to a unique class of light-responsive molecules, which are able to rotate 360° unidirectional (Koumura *et al.*, 1999; Koumura *et al.*, 2002; van Delden *et al.*, 2005). Powered by light, the central carbon-carbon double bond undergoes *trans-cis* isomerization, followed by the

energetically downhill process of thermal helix inversion. These photochemical and thermal steps induce a rotation of 180° of one half of the motor relative to the other. By repetition, the continuous unidirectional rotary motion is achieved. Importantly, the rotary direction is dictated by the stereogenic center(s) next to the central double bond, which cause the enantiomers to display opposite rotary directions with respect to each other.

To date, most molecular motors were studied in solutions or on surfaces, revealing that the surrounding environment, for example solvent viscosity, can affect the rotary motion of a molecular motor (Chen *et al.*, 2014; Kistemaker *et al.*, 2016). Compared to solvated systems, natural stimuli-responsive molecules often work in a more confined environment, such as proteins, where the isomerization processes can occur with special selectivity (Becker and Freedman, 1985; Smith, 2010). At the other extreme, a complete solid state can negatively influence the performance of many photo-responsive molecules (Naito *et al.*, 1991; Benard and Yu, 2000; Kobatake *et al.*, 2007; Harada *et al.*, 2010; Bushuyev *et al.*, 2013). In solid state, molecular motors often cease to rotate as they require a large geometrical structure change, which is blocked by the molecular confinement in solid state. Here we provide control of confinement parameters due to aggregation into bowl-shaped structures, which allows the study of molecular motor **1** under a wide range of confinement parameters.

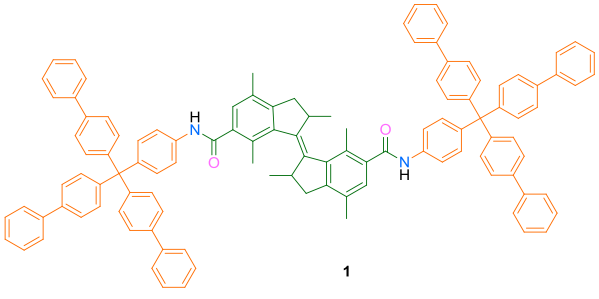

Figure 3-1: The chemical structure of bulky molecular motor 1. *The molecular motor contains a rotary core (green), two bulky aromatic groups (orange), and they are linked by amide groups (pink: oxygen atom; blue: nitrogen atom).*

In this work we not only demonstrate the consistent reproducibility to generate bowl-shaped spheres from various starting materials, but we also characterize the spheres under various solvent ratios by TEM, dynamic light scattering (DLS), fluorescence and nuclear magnetic resonance (NMR) spectroscopy. Furthermore we formulate and prove a general theory on both driving mechanism and particle nature. Lastly, we apply this system to a novel

molecular motor **1** and demonstrate the effect of confinement on its photo-physical as well as its rotary behavior.

2 Results and discussion

2.1 Solvent mixing with several molecules

Several hydrophobic molecules (PS174, Nile Red, Styrofoam, PVC171 and molecular motor **1**) were tested to see if in general bowl-shaped particles can be obtained by first solubilizing the molecule in THF and subsequently mixing the solution with water. The results can be seen in Figure 3-2. After optimization of molecule concentration and volume fraction of water (fw), the desired morphology was obtained through this method for all tested molecules.

In addition to THF-water, two other mixable solvents were tested: tertiary-butanol with water and chloroform with methanol. Although particles were formed, the holes in the exterior were found more rarely, indicating an influence of solvent-type on hole formation and/or size (Im *et al.*, 2005; Mai and Eisenberg, 2012). Im *et al.* (2005) briefly explored the approach from emulsion droplets of PMMA pellets solubilized in toluene prior to adding the non-mixable solvent water. Due to lack of mixability, multiple steps are needed: vortexing, addition of sodium styrene sulfonate as a surfactant, freezing in liquid nitrogen and finally solvent evaporation. Our results indicate that the presence of the hole can be achieved directly, without adding other materials and changing temperatures, when solvents are used that are mixable.

A different route to bowl-shaped spheres can be achieved by solvent evaporation (Vriezema *et al.*, 2003; Im *et al.*, 2005; Liu *et al.*, 2009; Alfonso *et al.*, 2010; Maity *et al.*, 2011). A particularly interesting method describes how solid, dispersed PS nano-particles in water were swollen by adding a non-mixing good solvent (toluene or styrene) (Im *et al.*, 2005). The swollen particles were frozen in liquid nitrogen and controlled temperature increase to evaporate the solvent led to the formation of temperature- and solvent-dependent, controllable holes. We tested this route using water-dispersed Latex (90 nm and 176 nm) and adding 50% THF. Surprisingly, the holes appeared immediately and no further steps were needed (Figure 3-3). The spheres display both uniformity in particle- and hole-size. Furthermore, DLS measurements indicate that the

bowl-shaped derivatives are swollen with respect to their precursor latex spheres.

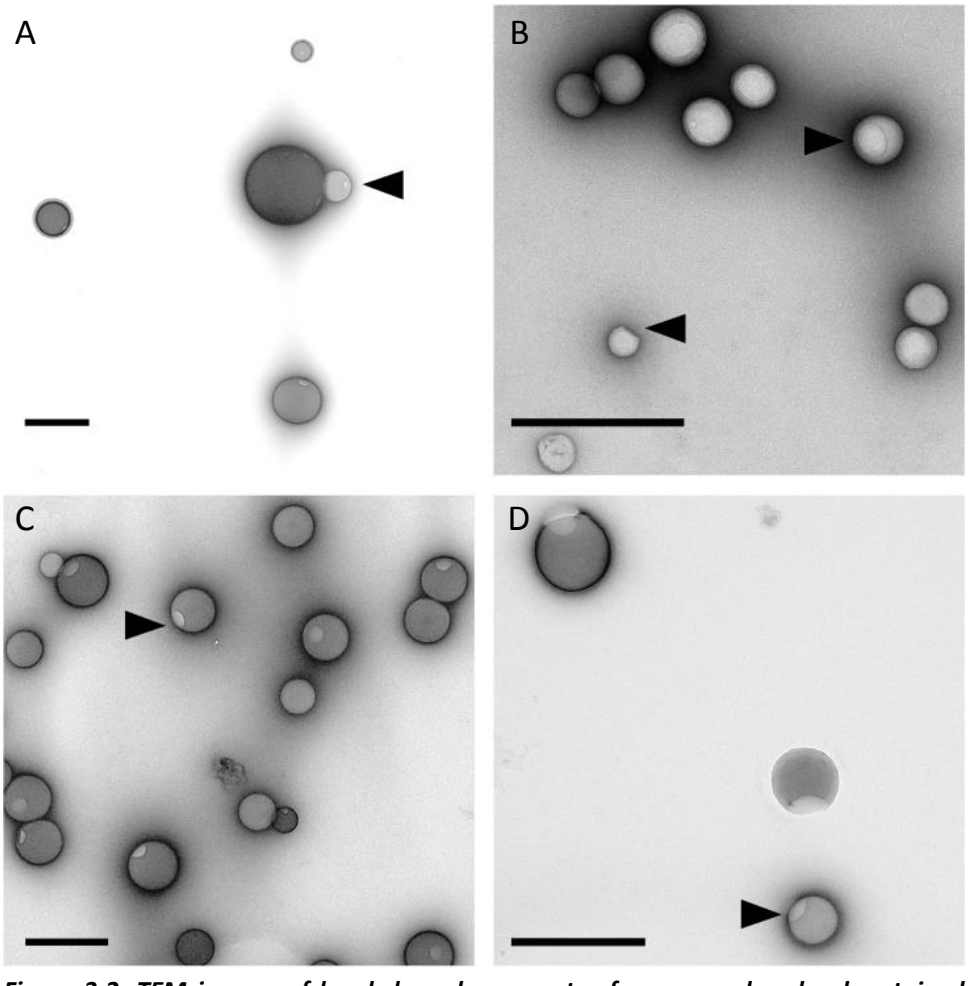

Figure 3-2: TEM images of bowl-shaped aggregates from several molecules stained with 2% UAc. *Reported are the starting concentration of the molecule in THF prior to mixing with water and the THF-water volume ratio after mixing, which were optimized for each sample.* ***A****) 1 mg/ml PS174 in THF at 50% fw.* ***B****) 0.5 mg/ml Nile Red at 75% fw.* ***C****) 0.5 mg/ml Styrofoam in 50% fw.* ***D****) 0.5 mg/ml PVC17 at 66% fw. Scale bars represent 500 nm and arrows indicate examples of holes in the exterior.*

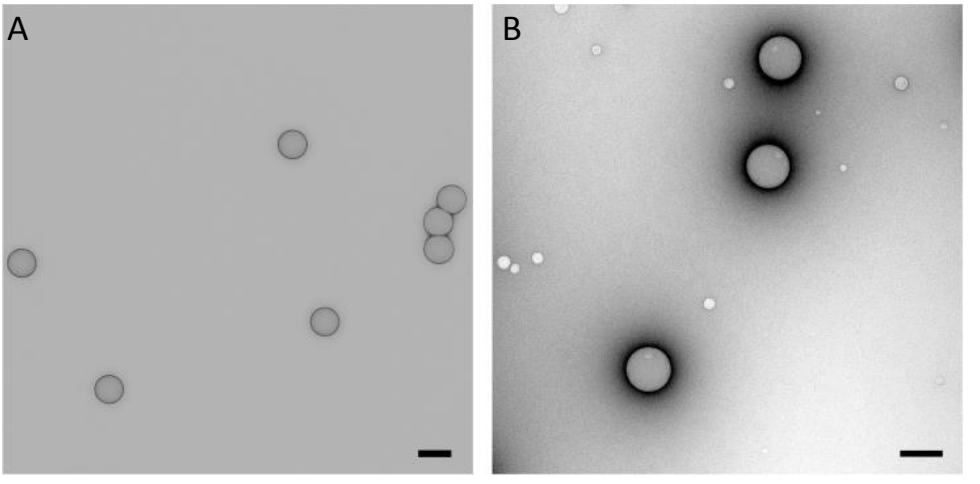

Figure 3-3: TEM images of Latex spheres of 176 nm (Ted Pella) (A) and with 50 volume% added THF (B). *Scale bars represent 200 nm.*

2.2 Characterization of the particles

2.2.1 Stability and size

In order to determine the nature of the particles, the spheres from the rotary motor were imaged using three different TEM preparation techniques: drying, negative staining and cryo-TEM (Figure 3-4) (Franken *et al.*, 2017). As can be observed, the hole in the exterior is visible in all three images and there is no apparent deformation, demonstrating that the particles are extremely stable and that the dent is not formed by dehydration or the TEM preparation method, but present in solution. Therefore the particles are either solid or very viscous. From the dried and cryo-TEM images, it can be observed that, although there is a hole in the particles, the structures are not hollow.

In order to test the stability over time, molecular motor **1** was prepared using a 60% and 90% fw and left for 4 days (Figure 3-5). Comparing the morphology of the two preparations, it can be observed that at lower water content, proper bowl-shaped particles are visible, whereas the higher water content seems to yield only sporadically a bowl-shaped particle and more often droplet-like particles without dents, which are occasionally surrounded by a ring of solvent. Where time transforms the droplet-like structures into proper

dented particles when fixed with 90% water, the larger spheres that were created using only 60% water crystallized slowly in time.

Another distinct difference between the spheres at 60% and 90% fw is their difference in size. DLS data show that the particle size shrinks with increasing fw. At 60% fw, DLS indicates a particle radius of 392 nm with a polydispersity of 64%, whereas at 90% fw the radius is 130 nm with a polydispersity of 35%. The shrinking/swelling of the aggregates is reversible by adding water or THF, respectively.

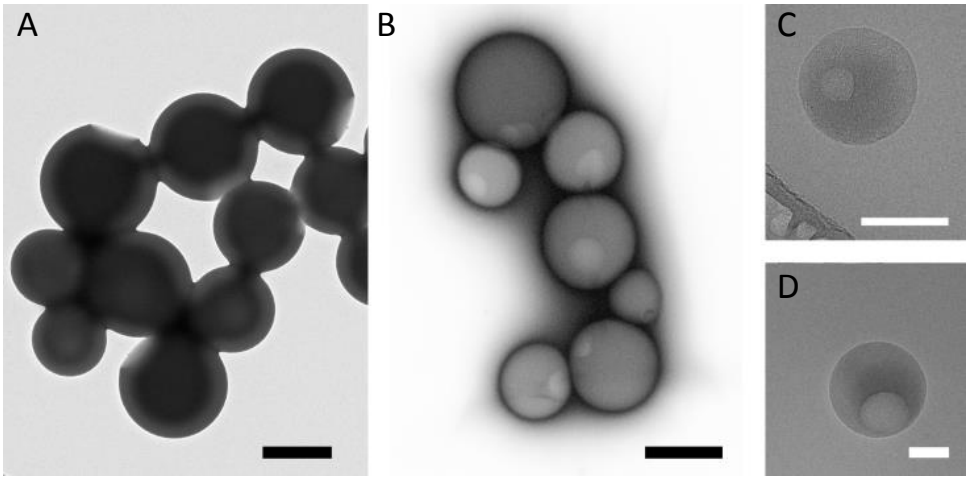

Figure 3-4: Spheres from the molecular motor 1 imaged by three TEM preparation techniques: drying (A), negative staining (B) and cryo-TEM (C and D). *Motor concentration was 10^{-4} M in THF. Panels **A** and **B** are imaged at 60% fw and **C** and **D** at 90% fw for reasons of particle size. Please be advised that drying alone is not a proper preparation method for these systems as also the drying of droplets can lead to dented spheres (Liu* et al.*, 2009; Alfonso* et al.*, 2010; Maity* et al.*, 2011; Yao* et al.*, 2014) and it cannot be distinguished whether the dents are formed upon drying or in solution. Scale bars represent 1 µm (black) and 100 nm (white), respectively.*

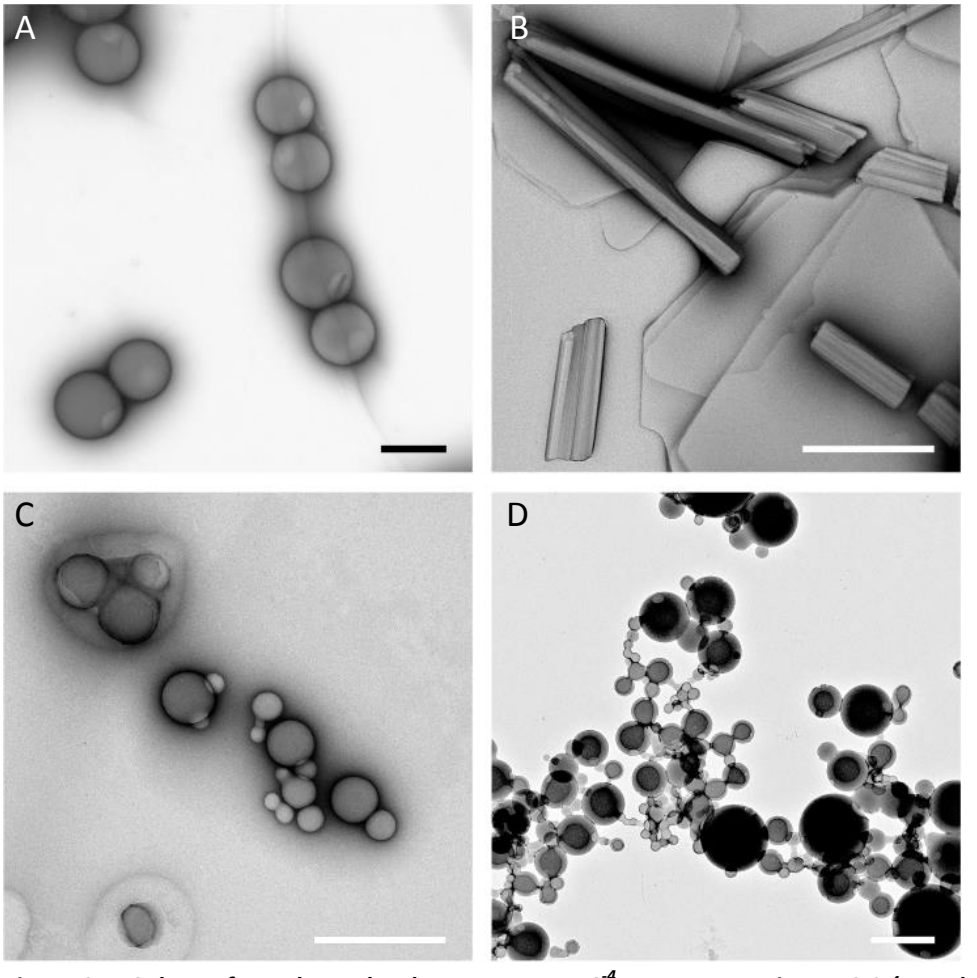

Figure 3-5: Spheres from the molecular motor 1 at 10^{-4} M concentration at 2:3 (A and B) and 1:9 THF:H2O (C and D), and their evolution over time. *Panels **B** and **D** are images of the same samples as **A** and **C**, but after 4 days of aging. Scale bars represent 1 µm (black) and 500 nm (white), respectively.*

2.2.2 Solvent content spheres: NMR

The extreme stability of the mature dented spheres allowed us to wash them by pelleting and resuspension in D_2O in order to remove all traces of THF and water from the surrounding medium prior to solubilizing the particles in d-chloroform for NMR. TEM observations confirm the unaffected nature of the spheres after washing (Figure 3-6). NMR confirms the presence of THF in the spheres and proofs their viscous nature.

The practices of washing, stirring overnight or dialysis to remove the initial solvent are commonly used (Zhang and Eisenberg, 1995; Riegel *et al.*, 2002; Riegel *et al.*, 2004; Yang *et al.*, 2010b; Mai and Eisenberg, 2012; Jiang *et al.*, 2014; Li *et al.*, 2014; Yao *et al.*, 2014). However our experiments show that in this, and likely other events, solvent remains inside the spheres even after extensive washing.

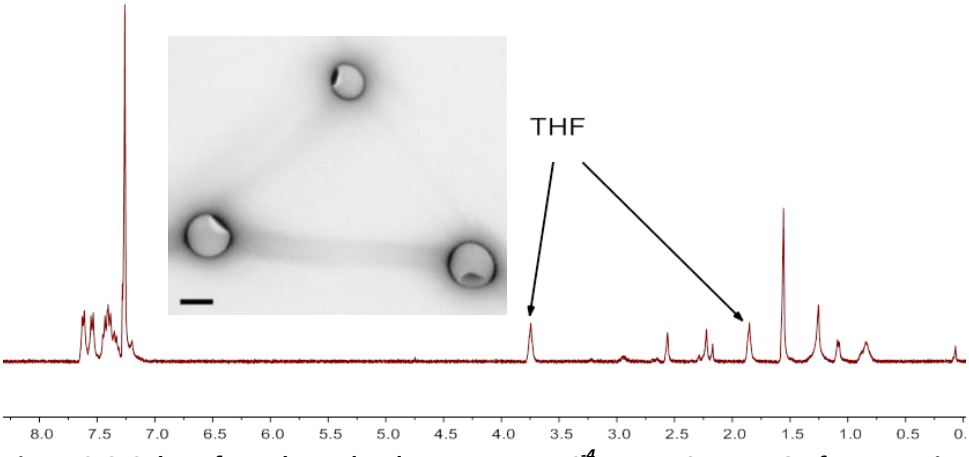

Figure 3-6: Sphere from the molecular motor 1 at 10^{-4} M at 1:9 THF:H_2O after excessive washing with H_2O (TEM image) and NMR results, where arrows point to peaks corresponding to THF. *Scale bar equals 200 nm.*

2.2.3 Hydrophobic effects: Nile Red fluorescence

In order to gain insight in the mechanism of bowl-shaped sphere formation, we used Nile Red fluorescence to monitor the polarity dependent fluorescence maximum in different solvent-water mixtures (Stuart *et al.*, 2005) (Figure 3-7). Measurements were started at pure solvent (methanol, ethanol (not shown for figure clarity), propanol, tert-butanol and THF) and water was added step-wise. Only in methanol-water the peak maximum keeps shifting linearly towards 660 nm (close to pure water (Stuart *et al.*, 2005)). In the other solvents at critical water content (CWC), the fluorescence spectrum suddenly widened, showing a second population of Nile Red that experienced a much lower polarity. The hydrophobic Nile red does not tolerate the polarity of the water and initiates phase separation into droplets. Expressing this in mole fraction rather than the more common mass fraction (*e.g.* (Zhang and Eisenberg, 1995; Shen and Eisenberg, 1999; Choucair and Eisenberg, 2003)) or volume fraction (*e.g.* (Im *et*

al., 2005; Mai and Eisenberg, 2012; Mei *et al.*, 2014)) suddenly shows that all solvents, except methanol, experience droplet formation at the same 95% mole ratio. This situation likely exists due to the infinitely diluted state of the Nile Red, which causes the water to only become polar at a critical 95 mol%, independent of the solvent (Blokzijl and Engberts, 1993). As soon as the concentration of Nile Red is increased for TEM measurements however, the CWC seems specific for the nature and concentration of the molecule and the nature of the initial solvent, rather than the water content. The fact that Nile Red does not cause precipitation into droplets in methanol underlines that not only the selective solvent, but also the good solvent quality plays a role.

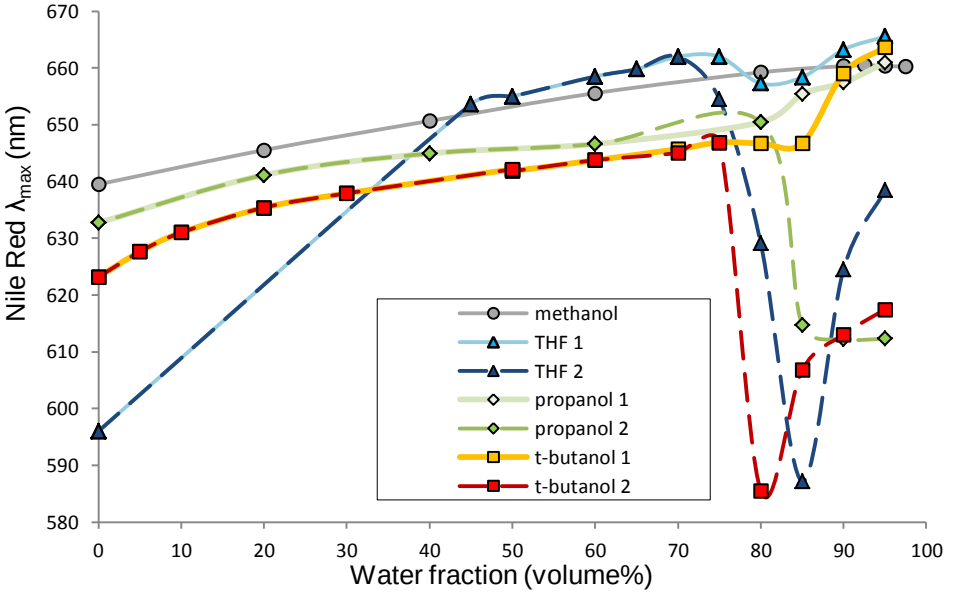

Figure 3-7: Nile Red fluorescence maxima, which change with polarity, of different solvent-water mixtures. *Water acts as precipitator for Nile Red in all mixtures except methanol-water, inducing low-polarity droplets. At the CWC, the fluorescence spectra cannot be explained with a single peak and are solved with convolution into two peaks (1 and 2), each peak representing a sub-population of the Nile Red.*

2.3 General mechanism and particle nature

Our experiments with the optimization of the formation of bowl-shaped particles indicate several general observations: i) the system depends on molecule, molecular concentration, solvent nature and solvent ratio; ii) with increased water content (immediate mixing, not gradual adding) the

morphology is first droplets, then bowl-shaped particles and then a mix of morphologies iii) time can mature the mixture to bowl-shaped spheres and allows precipitation at intermediate water content; iv) the bowl-shaped morphology can be achieved when starting from solid state in water. These observations and the numerous examples from the literature indicate a general mechanism for the formation of bowl-shaped particles.

The driving forces behind their formation can be found in the field of amphiphilic block-copolymer self-assembly, in particular in the work of Eisenberg *et al.*. Their results show high analogy to our own observations and identify the same parameters: molecular properties (*e.g.* (partial) hydrophobicity), molecular concentration and solvent types (Riegel *et al.*, 2002). In stark contrast to our observations stands the fact that the large majority (except for Riegel *et al.* (2002)) of their systems display various morphologies in response to altered solvent ratios. In those systems, each block of the amphiphilic molecules responds differently to the solvent changes. The corresponding molecular reorganization is thus driven by self-assembly and not independent of molecular design (Zhang and Eisenberg, 1995; Yu and Eisenberg, 1997; Shen and Eisenberg, 1999; Choucair and Eisenberg, 2003; Mai and Eisenberg, 2012). Besides self-assembly, Eisenberg *et al.* identify two key factors that govern the obtained morphologies: thermodynamics *versus* kinetics (Mai and Eisenberg, 2012). As long as the thermodynamics of reorganization are faster than the changes in water content, the structures are in equilibrium before they become kinetically frozen by high water content. Kinetical freezing of a structure at a certain stage of reorganization is achieved by adding a large amount of selective solvent (non-solvent) (Riegel *et al.*, 2002), which causes (part of) the molecular assembly to go below the glass transition temperature (T_g) (Zhang and Eisenberg, 1995).

Independent of the solvent mixture and molecular properties, addition of the selective solvent to a block copolymer in a solvent always induces the formation of so-called spherical micelle-like aggregates (MLAs) (Zhang and Eisenberg, 1995), at the CWC, prior to self-assembly under influence of the solvent mixture (Riegel *et al.*, 2002; Choucair and Eisenberg, 2003; Mai and Eisenberg, 2012). This initial 'micellation' can be distinguished from the self-assembly as the added selective solvent acts as a precipitant (Riegel *et al.*, 2002; Choucair and Eisenberg, 2003). This observation can be extrapolated to systems other than block copolymers, such as hydrophobic molecules. Since

hydrophobic molecules don't have partial, but complete repulsion from the selective solvent, it acts only as a precipitator, but does not induce self-assembly. It can be concluded that there is only one distinct difference between self-assembly of block copolymers in solvent mixtures and the formation of the bowl-shaped spheres: the spheres are kinetically frozen before self-assembly could take place. This can be the result of a high T_g of the molecule in relation to the solvents, or the slow kinetics of the combined system.

The fact that non-amphiphilic molecules can form (bowl-shaped) spheres disputes descriptions such as 'micellation', self-assembly, micelle or large compound micelle (LCM). Those terms imply reorganization as a consequence of molecular properties. Furthermore, reported TEM images, particle sizes and polydispersity in relation to molecular design often do not match the interpretation of an organized structure. Therefore, the correctness of this interpretation is debatable. This is true also for several amphiphilic molecules, since weak amphiphiles may have slow thermodynamics, reaching a kinetically frozen state prior to self-assembly. It would not be surprising if many currently described LMCs are in fact closely related to the bowl-shaped spheres and lack molecular organization.

We propose a mechanism of formation of bowl-shaped spheres that does not include self-assembly and provides new insights into the nature of the spheres and their derivatives (Figure 3-8). Upon addition of a critical amount of selective solvent, initial precipitation of the material occurs into amorphous, unorganized droplets of the molecule in initial solvent. Their viscosity can vary depending on the properties of the initial solvent (plasticizer effect) and the starting concentration of the molecule. Pressure from the selective solvent causes the shrinking or the droplets by release of solvent (cooling effect). Depending on the T_g of the molecule (in the initial solvent), its concentration and the amount of selective solvent, the exterior of the droplet hardens, whereas the inside remains fluid. Initially, the extruded solvent surrounds the spheres, but the limitless mixability of the two solvents washes the sphere. Until equilibrium is reached, the solvent pressure causes continued release of solvent, but as the droplet exterior is less permeable, the dent in the particle is formed as the solvent is extruded through the weakest part of the glass-shell. At this stage, the balance between interior fluidity under plasticizer strength against increase of T_g due to the unfavorable medium allows the dented spheres to reorganize over longer time scales. The more selective solvent is added, the

stronger the sphere holds on to the solvent, slowing down the exchange of solvent with the medium and ultimately reversing it. At large amounts of selective solvent, further compression squeezes solvent through the dent, which is the weakest part of the shell. Similar as at the initial stage of precipitation into droplets, the dented spheres are highly attracted to the solvent, which results in a mix of morphologies: spheres, usually with dents, that can be free or have droplets in the dents or surrounding them completely. Depending on the exact balance of all components, the latter situation can stabilize over time or revert to a droplet state. Washing with selective solvent will stabilize the dented spheres. In contrast to the method described by Im *et al.* (2005), this mechanism is highly dependent on the mixability of the two solvents and the dented spheres that are generated are not necessarily solid due to the plasticizing effect of internal solvent.

In summary: increase of the T_g by the non-solvent causes the droplets to shrink, which leads to the solidification of the exterior. As the exterior shrinks faster than the interior, the pressure increases until the point that the shell bursts, leaving a hole in the side of the glass-like droplet. As proof of principle of the proposed mechanism, we froze bath beads in liquid nitrogen to create bowl-shaped particles (Figure 3-9 and Supplementary Movie 1).

From literature, it can be gathered that evaporation of solvent from the spheres and shrinking by cooling through non-solvent yield the same result, which is understandable since evaporation also starts at the exterior of the spheres, ultimately yielding the same pressure from shrinking.

All our experiments, as well as the proposed mechanism of formation, indicate an asymmetric particle morphology, a shell-core particle with an internal gradient from a fluid interior to a glasslike exterior. The facts that dented spheres can be reached starting from the solid state in water by addition of THF and that dented spheres are formed from the 90% water sample over longer timescales indicate that the dented spheres represent a stable equilibrium. This equilibrium as well as the speed with which it is reached shift under influence of solvent types, solvent ratio, molecule type and molecule concentration. Although not further explored, we propose that temperature also plays a crucial role.

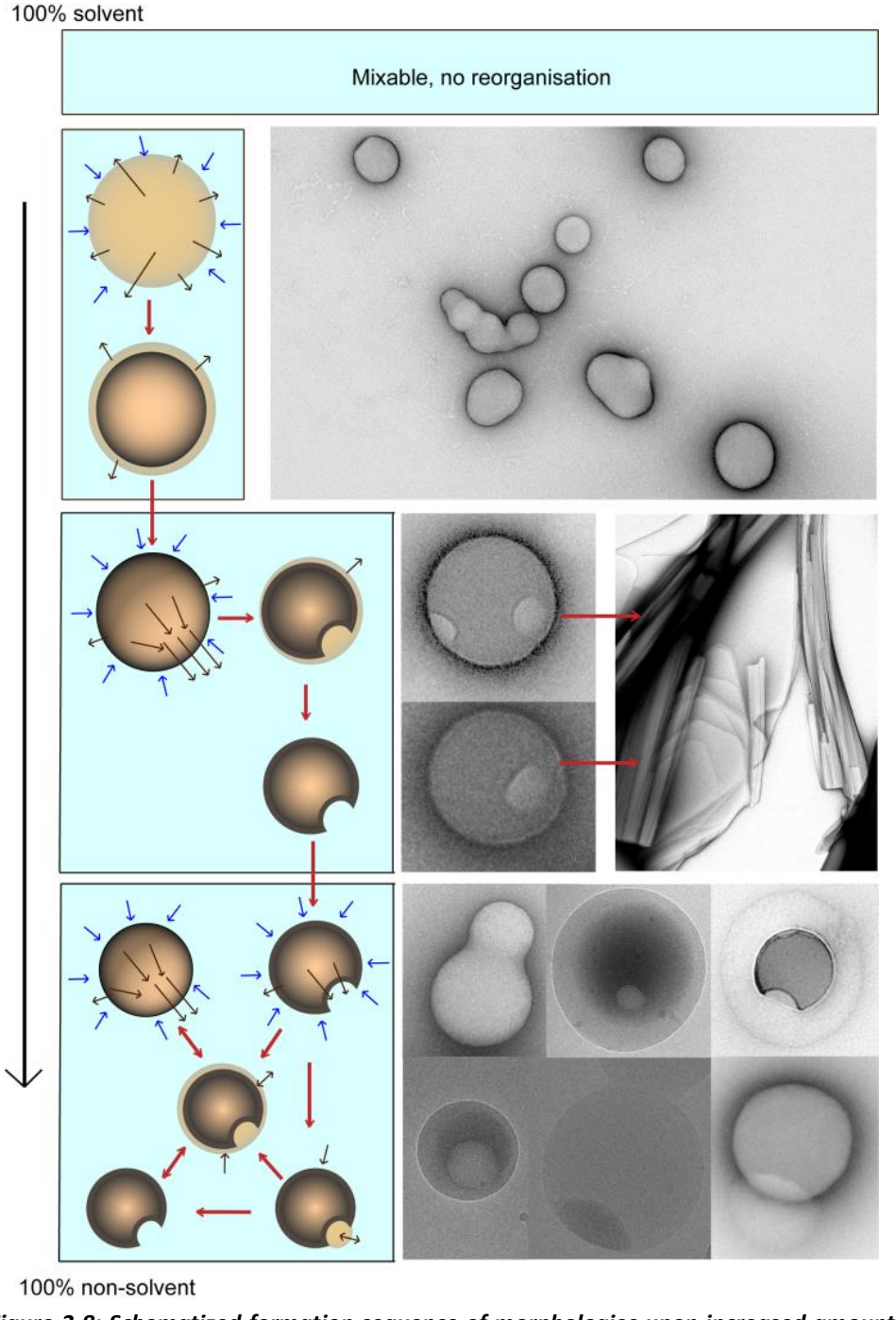

Figure 3-8: Schematized formation sequence of morphologies upon increased amount of selective solvent (non-solvent), starting from droplets to dented spheres to a mixture of different morphologies that have a balanced relation with the two solvents.

Figure 3-9: As proof of principle to the formation of dented spheres from droplets and lowering the T_g, bath beads were frozen in liquid nitrogen. *Under the pressure of the cooling of the exterior of the beads the shell bursts and a dent is formed. See also Supplementary Movie 1.*

2.4 Loading and other applications

While most experiments on loading of the particles have been conducted under the assumption that they are vesicles or polymersomes (Vriezema *et al.*, 2003; Vriezema *et al.*, 2007; van Dongen *et al.*, 2009), the idea to co-precipitate compounds into the spheres has been shown to work (Maity *et al.*, 2011). Although not vesicular, the presence of solvent in the reported particles provides an excellent platform for utilization. It is a compelling concept to use the spheres as nano-reactors, as they would provide an alternative environment compared to the bulk solvent. Considering the nature of the spheres, challenges lay in the optimization of the exhaustive amount of solvent combinations, molecules and concentrations, such that reaction components and products are able to cross the glass shell of the loaded particles, while the reactor remains enclosed in the sphere. Additionally, solvent and molecule type may provide

control over the dent-size (Im *et al.*, 2005) and thus exposed surface area, which may influence loading flux and reaction speed.

Other uses may be found in the method itself, using it as a precipitator or as a starting mechanism for crystallization. Furthermore, the extreme stability of the particles at higher water content makes that the particles can be successfully washed and selected by pelleting through size-exclusion membranes. An intriguing application could be de decoration or the particle surface (van Dongen *et al.*, 2009) using for example amphiphiles.

Lastly we found accounts of solvent mixing to induce aggregation and change fluorescent properties of luminogens (Wang *et al.*, 2012; Mei *et al.*, 2014). Although the morphology of the aggregates was not studied, the underlying mechanism of various states of confinement to alter fluorescence was adapted here: we used the dented spheres to control the freedom of movement of molecular motor **1**.

*2.4.1 Photochemical and thermal behavior of molecular motor **1** in solution*

The rotary behavior of the bulky molecular motor **1** was investigated in solution. Figure 3-10A describes the 360° unidirectional rotary cycle which includes two photo-isomerization and two thermal isomerization steps. Upon irradiation with 312 nm UV light, *trans*-stable **1** undergoes *trans-cis* isomerization, yielding the unstable isomer. This is indicated by the downfield shift of the aliphatic ring protons in the ^{1}H NMR spectra (Figure 3-10C). ^{1}H NMR shows that in its photo-stationary state (PSS), the ratio between the two isomers is 95% *cis*-unstable **1** and 5% *trans*-stable **1**. Circular Dichroism (CD) spectroscopy on enantiopure *trans*-stable **1** also confirms this light-triggered *trans-cis* isomerization process (Figure 3-10B).

Conducting subsequent thermal helix inversion by heating *cis*-unstable **1** at 60 ^{o}C for 2h yields the stable *cis*- isomer. The upfield shifts of all the aliphatic ring protons in the ^{1}H NMR spectra confirmed the formation of *cis*-stable **1**. Importantly, this thermal process is the rate-determining step and its thermodynamic parameters were investigated with a kinetic UV/vis study, which indicate the standard Gibbs energy of activation and the half-life of cis-unstable **1** to be 102.2±4.2 kJ•mol^{-1} and 26 h at 298.15 K respectively (Figure 3-11).

The high effectiveness of the photo-isomerization and the parameters of the thermal conversion step coincide with other first generation molecular motors with amide linkers (Zhao *et al.*, 2015a), showing that the bulky groups do not interfere with the motor rotation. This lack of steric hindrance is due to the relative flexibility of the amide linker, which allows both bulky groups to point away from each other.

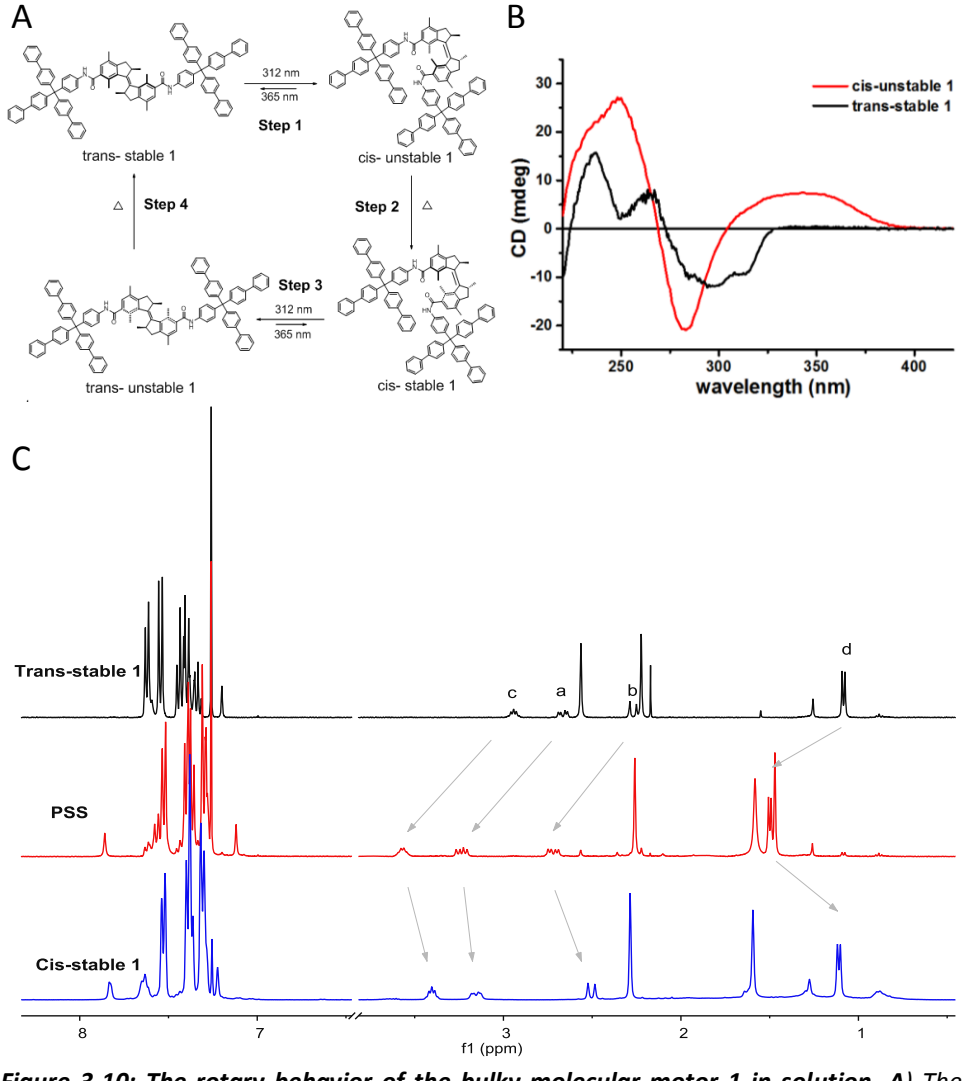

Figure 3-10: The rotary behavior of the bulky molecular motor 1 in solution. A*) The schematic 360° rotary cycle starting from the trans-stable* ***1****. B) CD characterization of step 1 in HF ([1]= 10^{-5} M). C) The 1H NMR spectra of trans-stable* ***1****, its PSS by irradiating with 312 nm UV light, and the subsequent cis-stable* ***1*** *by heating at 50 °C for 12 h (the solvent is d-chloroform).*

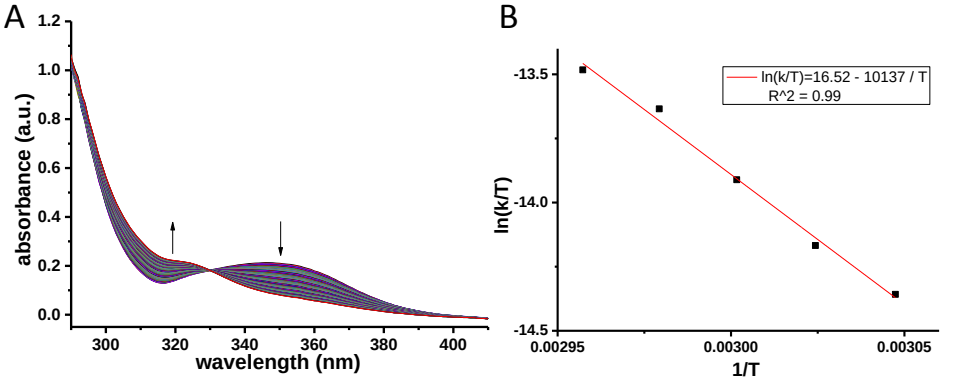

C

Δ‡Ho (kJ * mol $^{-1}$)	Δ‡So (J * mol^{-1} * K^{-1})	Δ‡Go (kJ * mol^{-1})	$t_{1/2}$ (h)
84.3±4.2	-60.2±5.5	102.2±4.2	26

Figure 3-11: Kinetic measurements of the thermal isomerization step 2 in THF. A) *UV/vis spectral changes during heating at 55 °C.* ***B)*** *The linear fitting of ln (k/T) by 1/T using Erying equation:*

$$\ln\frac{k}{T} = \frac{-\Delta H^{\ddagger}}{R}\cdot\frac{1}{T} + \ln\frac{k_{\mathrm{B}}}{h} + \frac{\Delta S^{\ddagger}}{R}$$

The rate constants of the first-order decay k were obtained from equation A/Ao= e^{-kt}, at 55 °C, 575 °C, 60 °C, 62.5 °C, and 65 °C. ***C)*** *The calculated standard enthalpy Δ‡Ho, entropy Δ‡So, Gibbs free energy Δ‡Go of activation, and the half-life of cis-unstable* ***1*** *at 298.15 K.*

2.4.2 In situ *photo-switchable aggregation-induced emission*

In the solid state, both the photochemical and thermal isomerization pathways of **1** are blocked. Due to the tight packing in the solid state, there is not enough space for conformational rearrangement. An intermediate state of confinement can be found in the bowl-shaped aggregates. Use of solvent/non-solvent mixing (THF-H_2O) in different ratios gave control over the confinement of motor **1** and concomitantly its rotary behavior. Concentration of the motor into bowl-shaped aggregates demonstrated aggregation-induced emission (AIE) properties of the motor upon UV irradiation (Luo *et al.*, 2001; Wang *et al.*, 2012; Mei *et al.*, 2014; Mei *et al.*, 2015; Zhao *et al.*, 2015b). Both the photo-physics and photo-chemistry of molecular motor **1** in the confined space were investigated.

As shown in Figure 3-12A, trans-stable **1** displays no fluorescence in pure THF. When fw is increased to ~60 %, bowl-shaped particles are formed (Figure

3-5) and the motor shows fluorescence, which intensifies as the water concentration increases. In other words, the *trans*-stable isomer of the bulky molecular motor is AIE active. Similar AIE behaviors are also displayed by the other isomers (Figure 3-12B). The fluorescence quantum yield is moderate: for cis-unstable, it increases from 0.3% at fw = 0 to 2.7% at fw = 90 %. Notably, the purplish blue fluorescence of *trans*-stable **1** (λ_{max} 482 nm) shifts to greenish blue for the *cis*-unstable **1** (λ_{max} 490 nm) (Figure 3-12). This difference results from the different electronic structures of trans-stable and cis-unstable isomers. There is no difference in morphology and size of the aggregates from different isomers.

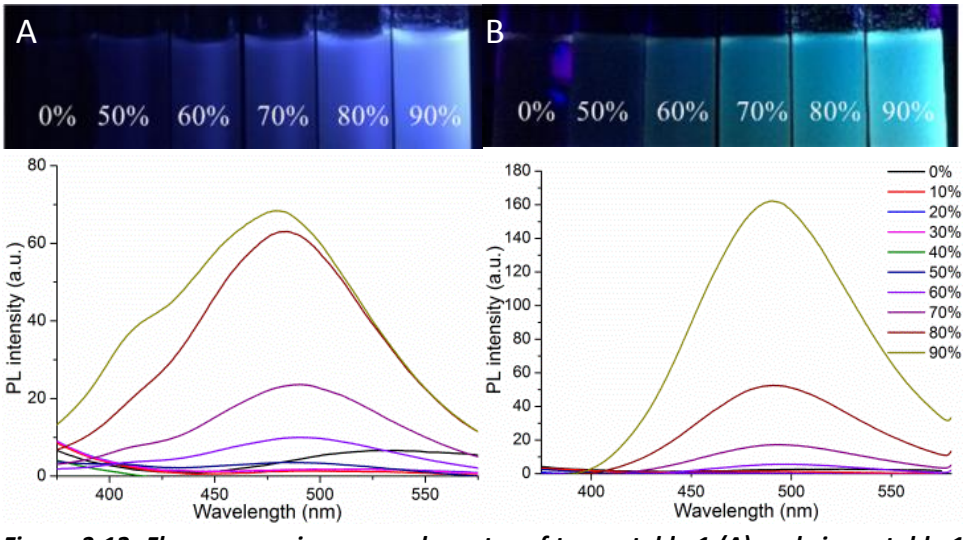

Figure 3-12: Fluorescence images and spectra of trans-stable 1 (A) and cis-unstable 1 (B) in aggregates formed from THF/water with different water fraction fw. *The total concentration of 1 in the mixtures was maintained at 10^{-4} M and λ_{ex} = 300 nm.*

To determine the photochemical isomerization process *in situ* in the aggregates, the fluorescence of *trans*-stable **1** in fw=90% was monitored over time while irradiating with 300 nm UV light (Figure 3-13A). While morphologically the aggregates do not change, the broad absorption band gradually becomes narrower accompanied with a disappearance of the shoulder and a slight red-shift of the whole spectrum, which indicates the formation of *cis*-unstable **1**. Moreover, the clear isosbestic point demonstrates that there is no occurrence of other species during the irradiation. The photo-isomerization process is also confirmed by CD using enantiopure compound **1** (Figure 3-13B).

The aggregates of *trans*-stable **1** are CD-silent at >350 nm, however, a positive Cotton effect emerges at 362 nm upon irradiation with UV, which confirms the generation of *cis*-unstable **1**. In contrast to the CD spectra in solution, there is a red-shift of the Cotton effect in aggregated state mainly due to light scattering of the aggregates. To confirm the photochemical conversion, ^{1}H NMR analysis was used. After reaching its PSS at fw = 90%, a ratio of 31% *trans*-stable **1** and 69% *cis*-unstable **1** was established. Decreasing fw led to faster reach of PSS as well as higher conversion-rates, *e.g.* at fw = 60% the PSS ratio is similar to that in solution.

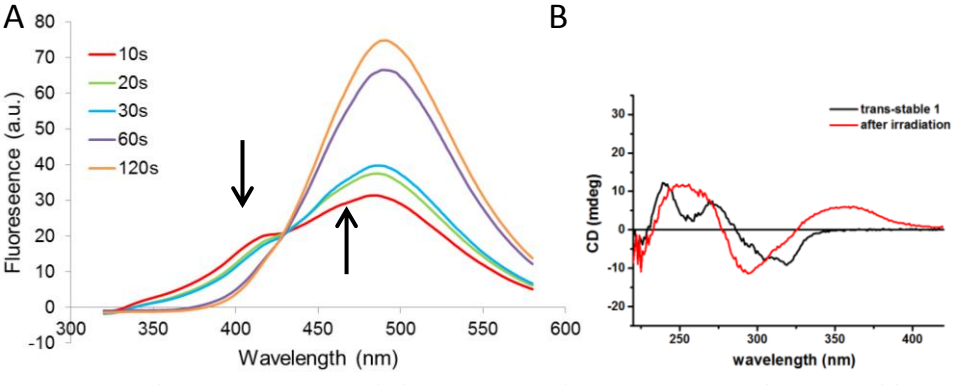

Figure 3-13: Fluorescence spectral change on irradiating aggregated trans-stable 1 in THF: water = 1: 9, [1] = 10^{-5} M (A) and CD spectral change, [1] = 10^{-5} M (B).

2.4.3 Thermal relaxation in the confined environment

The thermal helix inversion performance of molecular motor **1** in aggregates was also studied. Initially, *trans*-stable **1** was irradiated to its PSS in THF, generating the *cis*-unstable isomers. Then aggregation was induced by adding water to reach f_w = 90%. After prolonged heating, ^{1}H NMR analysis showed absence of *cis*-stable **1**, indicating that the thermal helix inversion step was totally blocked in the aggregates.

While at lower water content, both helix inversion and *cis-trans* isomerization occur as in solution, at 90% fw this is not the case. Upon irradiation with UV light of *trans*-stable **1** aggregates, a ratio of 31% *trans*-stable and 69% *cis*-unstable isomers was established. To our surprise, the ratio changed to 56% *trans*-stable and 44% *cis*-unstable isomers after heating, while there was no presence of *cis*-stable **1**. This phenomenon indicates that, while

the helix inversion step is blocked, *in situ* generated *cis*-unstable isomers can undergo a thermal *cis-trans* isomerization. This process has a much higher energy barrier in the molecularly dissolved state than the thermal helix inversion process. Apparently, the increased confinement allows the rotary motor to switch back to regenerate *trans-stable* **1**. This observation will be further investigated.

3. Conclusions

In summary, we showed how and why weak amphiphiles and hydrophobic molecules are formed into bowl-shaped particles under influence of solvent mixing (and evaporation). The adding of a non-solvent induces aggregation into droplets which, under influence of the non–solvent, are compressed and hardened from the exterior, while the interior is untouched by the non-solvent and does not shrink, leading ultimately to the bursting of the shell and formation of a hole in the spherical aggregate. We undisputedly demonstrate that the spheres are neither hollow, vesicular nor micellar. The dense spheres with a fluid interior and a glass-like shell can be made from a multitude of materials, such that this aggregation behavior should not be termed self-assembly, but solvent-driven assembly.

Furthermore, the aggregates can shrink and swell reversibly by adding non-solvent or solvent respectively, giving control over the strength of confinement inside the spheres. As an application, we use this to control the rotary behavior of the bulky molecular motor **1** by influencing the photochemical and thermal isomerization processes. Upon confinement, the energy barriers that determine the rotary motion of the motor change, blocking *cis*-stable **1** isomerization, while allowing a thermal reversion *cis*-unstable to *trans*-stable state. In aggregated state, molecular motor **1** shows photo-switchable AIE behavior as the fluorescence can switch from purplish blue to greenish blue.

Although bowl-shaped spheres are not vesicular, we expect that this elucidation of their actual nature and the general mechanism of their formation will open the door to a wide range of applications that use their controllable size and their fluid interior that allows loading, compartmentalization and confinement.

4. Materials and methods

4.1 Synthesis of bulky first generation molecular motor 1

We chose the first generation molecular motor as building block, because of its high quantum efficiency. To work in a more confined environment, the detrimental packing of central olefin needed to be prohibited. By attaching two bulky 4,4'',4''''-(p-tolylmethanetriyl)tri-1'''',1''''''-biphenyl groups to each half of the molecular motor with an amide linker, the rotary core was shielded. The synthesis of the rotary motor is shown in Figure 3-14.

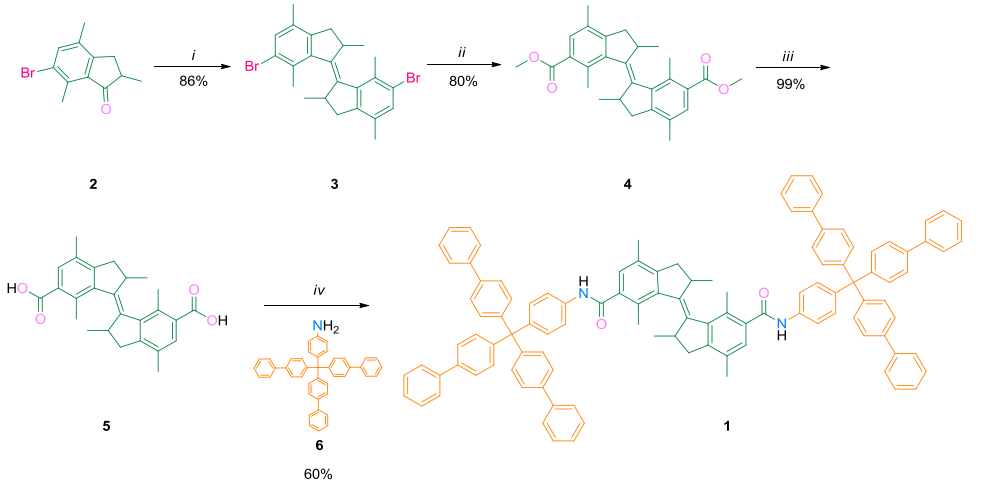

Figure 3-14: Synthesis of bulky molecular motor 1. *i) Zink powder,$TiCl_4$, reflux, 3d; ii) $Pd(dppp)_2Cl_2$, K_2CO_3, MeOH, NMP, CO(7.5 bar), 110 °C, 2d; iii) 1M aq. NaOH, MeOH, THF, 65 °C, 18h; iv) ① oxalyl chloride, DCM, THF, DMF, 0 °C, 1h; ② DCM, triethylamine, r.t., 18h.*

The synthesis of compound **1** was based on a well-established method (Naito *et al.*, 1991). It started with McMurry coupling of two identical cycloketone **2** to form the central olefin bond, giving the dibromo motor as a mixture of *trans*- and *cis*- isomers (*trans*-**3**:*cis*-**3** = 3:1). Palladium-catalyzed carbonylation introduced diester onto the motor and the two isomers were separated with a total yield of 80% (60% for *trans*-**4** and 20% for *cis*-**4**). The following hydrolysis resulted in the dicarboxylic acid with a nearly quantitative yield. After treatment with oxalyl chloride in THF and DCM as well as a catalytic amount of DMF, dicarboxylic acid 5 yielded a carbonyl chloride as an

intermediate, which was directly used in the next step of condensation with 4-(tri([1,1'-biphenyl]-4-yl)methyl)aniline to give the final product **1**.

4.2 Dynamic Light Scattering

DLS was performed using a Dynapro nanostar. The results were analyzed with dynamics software version 7, taking into account the viscosity of the THF-H_2O mixtures (Hao *et al.*, 2010).

4.3 Fluorescence measurements

Nile Red fluorescence was measured on an SPF-500c spectrofluorimeter (SLM Aminco) or a PTI International type C60/C-60 SE fluorimeter using an excitation wavelength of 490 nm. Fluorescent emission was measured from 510 to 700 nm at 5 or 1 nm intervals. The Nile Red emission maximum (λ max) was calculated using a log-normal fit (Stuart *et al.*, 2005).

4.4 NMR

To test whether THF remained inside the aggregates ^{1}H NMR was performed. The aggregates were prepared by adding 27 mL D_2O to the solution of 5 mg *trans*-stable **1** in 3 mL THF. The resulting mixture was then centrifuged (15.000 rpm, 10 min) to separate the spheres from the aqueous phase. To the isolated aggregates, D_2O (3 X 30 mL) was added, and the mixture was further sonicated and centrifuged until no THF was detected in D_2O by ^{1}H NMR. The washed aggregates were mounted into a NMR tube and dissolved with *d*-chloroform. NMR spectra were recorded using a Varian Mercury Plus, operating at 399.93 MHz.

4.5 TEM and cryo-TEM

TEM and cryo-TEM images were made using two electron microscopes depending on availability. The first was a Philips CM120 electron microscope (FEI, Eindhoven, The Netherlands) operated at 120 kV. The other was a Tecnai G2 20 Twin electron microscope (FEI, Eindhoven, The Netherlands) operated at 200 kV. Both microscopes are equipped with a LaB6 cathode and 4K slow-scan

CCD camera (Gatan, Pleasanton, CA, USA). Images were recorded using low-dose mode. Three microliters of the sample solution was pipetted on glow-discharged copper grid coated with a continuous carbon film for negative staining with 2% uranyl acetate or drying (stability experiments). For cryo-TEM, the sample was applied to holey carbon film (quantifoil 3.5/1) and plunge-frozen with a Vitrobot (FEI, Eindhoven, The Netherlands) in liquid ethane after blotting for 5 s. The specimen was then inserted into a cryo-transfer holder (Gatan model 626). Each micrograph was cropped and had adjustments of levels, brightness, and contrast in Adobe Photoshop CS6.

5. Acknowledgments

Our thanks to Dr. Anton Hofman for supplying us with the polymers (Figure 3-2), Prof. Dr. Katja Loos for valuable discussions and to Dr. Sander Wezenberg for discussion and proofreading the manuscript. This research is financed in part by the BioSolar Cells open innovation consortium, supported by the Dutch Ministry of Economic Affairs, Agriculture and Innovation (LEF).

6. References

Alfonso, I. Bru, M. Burguete, M. I. Garcia-Verdugo, E. and Luis, S. V., 2010. Structural Diversity in the Self-Assembly of Pseudopeptidic Macrocycles. Chemistry-a European Journal. Vol. 16 I. 4 p. 1246-1255.

Allen, T. M. and Cullis, P. R., 2013. Liposomal drug delivery systems: From concept to clinical applications. Advanced Drug Delivery Reviews. Vol. 65 I. 1 p. 36-48.

Becker, R. and Freedman, K., 1985. A Comprehensive Investigation of the Mechanism and Photophysics of Isomerization of a Protonated and Unprotonated Schiff-Base of 11-Cis-Retinal. Journal of the American Chemical Society. Vol. 107 I. 6 p. 1477-1485.

Benard, S. and Yu, P., 2000. New spiropyrans showing crystalline-State photochromism. Advanced Materials. Vol. 12 I. 1 p. 48-50.

Berzin, F. Vergnes, B. and Delamare, L., 2001. Rheological behavior of controlled-rheology polypropylenes obtained by peroxide-promoted degradation during extrusion: Comparison between homopolymer and copolymer. Journal of Applied Polymer Science. Vol. 80 I. 8 p. 1243-1252.

Blokzijl, W. and Engberts, J., 1993. Hydrophobic Effects - Opinions and Facts. Angewandte Chemie-International Edition. Vol. 32 I. 11 p. 1545-1579.

Brizard, A. Stuart, M. van Bommel, K. Friggeri, A. de Jong, M. and van Esch, J., 2008. Preparation of nanostructures by orthogonal self-assembly of hydrogelators and surfactants. Angewandte Chemie-International Edition. Vol. 47 I. 11 p. 2063-2066.

Bushuyev, O. S. Tomberg, A. Friscic, T. and Barrett, C. J., 2013. Shaping Crystals with Light: Crystal-to-Crystal Isomerization and Photomechanical Effect in Fluorinated Azobenzenes. Journal of the American Chemical Society. Vol. 135 I. 34 p. 12556-12559.

Chen, J. Kistemaker, J. C. M. Robertus, J. and Feringa, B. L., 2014. Molecular Stirrers in Action. Journal of the American Chemical Society. Vol. 136 I. 42 p. 14924-14932.

Choucair, A. and Eisenberg, A., 2003. Control of amphiphilic block copolymer morphologies using solution conditions. European Physical Journal E. Vol. 10 I. 1 p. 37-44.

Cordier, P. Tournilhac, F. Soulie-Ziakovic, C. and Leibler, L., 2008. Self-healing and thermoreversible rubber from supramolecular assembly. Nature. Vol. 451 I. 7181 p. 977-980.

Decher, G. 1997. Fuzzy nanoassemblies: Toward layered polymeric multicomposites. Science. Vol. 277 I. 5330 p. 1232-1237.

van Delden, R. ter Wiel, M. Pollard, M. Vicario, J. Koumura, N. and Feringa, B., 2005. Unidirectional molecular motor on a gold surface. Nature. Vol. 437 I. 7063 p. 1337-1340.

Denisov, I. Grinkova, Y. Lazarides, A. and Sligar, S., 2004. Directed self-assembly of monodisperse phospholipid bilayer nanodiscs with controlled size. Journal of the American Chemical Society. Vol. 126 I. 11 p. 3477-3487.

van Dongen, S. F. M. Nallani, M. Cornelissen, J. L. L. M. Nolte, R. J. M. and van Hest, J. C. M., 2009. A Three-Enzyme Cascade Reaction through Positional Assembly of Enzymes in a Polymersome Nanoreactor. Chemistry-a European Journal. Vol. 15 I. 5 p. 1107-1114.

Franken, L. E. Boekema, E. J. and Stuart, M. C. A., 2017. Transmission Electron Microscopy as a Tool for the Characterization of Soft Materials: Application and Interpretation. Advanced Science. p. 1600476-n/a.

Ganta, S. Devalapally, H. Shahiwala, A. and Amiji, M., 2008. A review of stimuli-responsive nanocarriers for drug and gene delivery. Journal of Controlled Release. Vol. 126 I. 3 p. 187-204.

Groeschel, A. H. Schacher, F. H. Schmalz, H. Borisov, O. V. Zhulina, E. B. Walther, A. and Mueller, A. H. E., 2012. Precise hierarchical self-assembly of multicompartment micelles. Nature Communications. Vol. 3 p. 710.

Grzelczak, M. Vermant, J. Furst, E. M. and Liz-Marzan, L. M., 2010. Directed Self-Assembly of Nanoparticles. Acs Nano. Vol. 4 I. 7 p. 3591-3605.

Hao, J. Cheng, H. Butler, P. Zhang, L. and Han, C. C., 2010. Origin of cononsolvency, based on the structure of tetrahydrofuran-water mixture. Journal of Chemical Physics. Vol. 132 I. 15 p. 154902.

Harada, J. Kawazoe, Y. and Ogawa, K., 2010. Photochromism of spiropyrans and spirooxazines in the solid state: low temperature enhances photocoloration. Chemical Communications. Vol. 46 I. 15 p. 2593-2595.

Hartgerink, J. Beniash, E. and Stupp, S., 2002. Peptide-amphiphile nanofibers: A versatile scaffold for the preparation of self-assembling materials. Proceedings of the National Academy of Sciences of the United States of America. Vol. 99 I. 8 p. 5133-5138.

He, Q. Ao, Y. Huang, Z. and Wang, D., 2015. Self-Assembly and Disassembly of Vesicles as Controlled by Anion-pi Interactions. Angewandte Chemie-International Edition. Vol. 54 I. 40 p. 11785-11790.

Im, S. Jeong, U. and Xia, Y., 2005. Polymer hollow particles with controllable holes in their surfaces. Nature Materials. Vol. 4 I. 9 p. 671-675.

Jiang, X. Jiang, X. Lu, G. Feng, C. and Huang, X., 2014. The first amphiphilic graft copolymer bearing a hydrophilic poly(2-hydroxylethyl acrylate) backbone synthesized by successive RAFT and ATRP. Polymer Chemistry. Vol. 5 I. 17 p. 4915-4925.

Jin, Y. Song, L. Wang, D. Qiu, F. Yan, D. Zhu, B. and Zhu, X., 2012. Synthesis and self-assembly of nonamphiphilic hyperbranched polyoximes. Soft Matter. Vol. 8 I. 39 p. 10017-10025.

Jochum, F. D. and Theato, P., 2013. Temperature- and light-responsive smart polymer materials. Chemical Society Reviews. Vol. 42 I. 17 p. 7468-7483.

Kistemaker, J. C. M. Lubbe, A. S. Bloemsma, E. A. and Feringa, B. L., 2016. On the Role of Viscosity in the Eyring Equation. ChemPhysChem. Vol. 17 I. 12 p. 1819-1822.

Kobatake, S. Takami, S. Muto, H. Ishikawa, T. and Irie, M., 2007. Rapid and reversible shape changes of molecular crystals on photoirradiation. Nature. Vol. 446 I. 7137 p. 778-781.

Koumura, N. Zijlstra, R. van Delden, R. Harada, N. and Feringa, B., 1999. Light-driven monodirectional molecular rotor. Nature. Vol. 401 I. 6749 p. 152-155.

Koumura, N. Geertsema, E. van Gelder, M. Meetsma, A. and Feringa, B., 2002. Second generation light-driven molecular motors. unidirectional rotation controlled by a single stereogenic center with near-perfect photoequilibria and acceleration of the speed of rotation by structural modification. Journal of the American Chemical Society. Vol. 124 I. 18 p. 5037-5051.

Li, G. Du, F. Wang, H. and Bai, R., 2014. Synthesis and self-assembly of carbazole-based amphiphilic triblock copolymers with aggregation-induced emission enhancement. Reactive & Functional Polymers. Vol. 75 p. 75-80.

Liu, B. (Ed.). 2016. Aggregation-Induced Emission. [Special Issue]. Small. Vol. 12 I. 47 p. 6419-–6632.

Liu, X. Liu, J. and Jiang, M., 2009. Spontaneous Self-Assembly of a Mono-Component Polyimide Bearing Terminal Hydrogen-Bonding Sites in a Single Solvent. Macromolecular Rapid Communications. Vol. 30 I. 11 p. 892-896.

Luo, J. Xie, Z. Lam, J. Cheng, L. Chen, H. Qiu, C. Kwok, H. Zhan, X. Liu, Y. Zhu, D. and Tang, B., 2001. Aggregation-induced emission of 1-methyl-1,2,3,4,5-pentaphenylsilole. Chemical Communications. I. 18 p. 1740-1741.

Mai, Y. and Eisenberg, A., 2012. Self-assembly of block copolymers. Chemical Society Reviews. Vol. 41 I. 18 p. 5969-5985.

Maity, S. Jana, P. Maity, S. K. and Haldar, D., 2011. Fabrication of Hollow Self-Assembled Peptide Microvesicles and Transition from Sphere-to-Rod Structure. Langmuir. Vol. 27 I. 7 p. 3835-3841.

Mei, J. Hong, Y. Lam, J. W. Y. Qin, A. Tang, Y. and Tang, B. Z., 2014. Aggregation-Induced Emission: The Whole Is More Brilliant than the Parts. Advanced Materials. Vol. 26 I. 31 p. 5429-5479.

Mei, J. Leung, N. L. C. Kwok, R. T. K. Lam, J. W. Y. and Tang, B. Z., 2015. Aggregation-Induced Emission: Together We Shine, United We Soar! Chemical reviews. Vol. 115 I. 21 p. 11718-11940.

Mitra, A. Panda, D. K. Corson, L. J. and Saha, S., 2013. Controllable self-assembly of amphiphilic macrocycles into closed-shell and open-shell vesicles, nanotubes, and fibers. Chemical Communications. Vol. 49 I. 41 p. 4601-4603.

Mura, S. Nicolas, J. and Couvreur, P., 2013. Stimuli-responsive nanocarriers for drug delivery. Nature Materials. Vol. 12 I. 11 p. 991-1003.

Naito, T. Horie, K. and Mita, I., 1991. Photochemistry in Polymer Solids .11. the Effects of the Size of Reaction Groups and the Mode of Photoisomerization on Photochromic Reactions in Polycarbonate Film. Macromolecules. Vol. 24 I. 10 p. 2907-2911.

Nicolas, J. Mura, S. Brambilla, D. Mackiewicz, N. and Couvreur, P., 2013. Design, functionalization strategies and biomedical applications of targeted biodegradable/biocompatible polymer-based nanocarriers for drug delivery. Chemical Society Reviews. Vol. 42 I. 3 p. 1147-1235.

Park, C. Yoon, J. and Thomas, E., 2003. Enabling nanotechnology with self assembled block copolymer patterns. Polymer. Vol. 44 I. 22 p. 6725-6760.

Riegel, I. Eisenberg, A. Petzhold, C. and Samios, D., 2002. Novel bowl-shaped morphology of crew-cut aggregates from Amphiphilic block copolymers of styrene and 5-(N,N-diethylamino)isoprene. Langmuir. Vol. 18 I. 8 p. 3358-3363.

Riegel, I. de Bittencourt, F. Terrau, O. Eisenberg, A. Petzhold, C. and Samios, D., 2004. Dynamics and structure of an amphiphilic triblock copolymer of styrene and 5-(N,N-diethylamino) isoprene in selective solvents. Pure and Applied Chemistry. Vol. 76 I. 1 p. 123-131.

Schneider, J. Pochan, D. Ozbas, B. Rajagopal, K. Pakstis, L. and Kretsinger, J., 2002. Responsive hydrogels from the intramolecular folding and self-assembly of a designed peptide. Journal of the American Chemical Society. Vol. 124 I. 50 p. 15030-15037.

Shen, H. and Eisenberg, A., 1999. Morphological phase diagram for a ternary system of block copolymer PS310-b-PAA(52)/dioxane/H2O. Journal of Physical Chemistry B. Vol. 103 I. 44 p. 9473-9487.

Smith, S. O. 2010. Structure and Activation of the Visual Pigment Rhodopsin. Annual Review of Biophysics, Vol 39. Vol. 39 p. 309-328.

Stuart, M. A. C. Huck, W. T. S. Genzer, J. Mueller, M. Ober, C. Stamm, M. Sukhorukov, G. B. Szleifer, I. Tsukruk, V. V. Urban, M. Winnik, F. Zauscher, S. Luzinov, I. and Minko, S., 2010. Emerging applications of stimuli-responsive polymer materials. Nature Materials. Vol. 9 I. 2 p. 101-113.

Stuart, M. van de Pas, J. and Engberts, J., 2005. The use of Nile Red to monitor the aggregation behavior in ternary surfactant-water-organic solvent systems. Journal of Physical Organic Chemistry. Vol. 18 I. 9 p. 929-934.

Sun, Y. and Liu, W., 2012. Synthesis and properties of cross-linkable block copolymer end-capped with 2, 2, 3, 4, 4, 4-hexafluorobutyl methacrylate. Journal of Polymer Research. Vol. 19 I. 1 p. 9768.

Toohey, K. S. Sottos, N. R. Lewis, J. A. Moore, J. S. and White, S. R., 2007. Self-healing materials with microvascular networks. Nature Materials. Vol. 6 I. 8 p. 581-585.

Torchilin, V. P. 2007. Micellar nanocarriers: Pharmaceutical perspectives. Pharmaceutical research. Vol. 24 I. 1 p. 1-16.

Tzoganakis, C. Vlachopoulos, J. and Hamielec, A., 1988. Production of Controlled-Rheology Polypropylene Resins by Peroxide Promoted Degradation during Extrusion. Polymer Engineering and Science. Vol. 28 I. 3 p. 170-180.

Vriezema, D. M. Hoogboom, J. Velonia, K. Takazawa, K. Christianen, P. C. M. Maan, J. C. Rowan, A. E. and Nolte, R. J. M., 2003. Vesicles and Polymerized Vesicles from Thiophene-Containing Rod–Coil Block Copolymers. Angewandte Chemie International Edition. Vol. 42 I. 7 p. 772-776.

Vriezema, D. M. Garcia, P. M. L. Oltra, N. S. Hatzakis, N. S. Kuiper, S. M. Nolte, R. J. M. Rowan, A. E. and van Hest, J. C. M., 2007. Positional assembly of enzymes in polymersome nanoreactors for cascade reactions. Angewandte Chemie-International Edition. Vol. 46 I. 39 p. 7378-7382.

Wang, J. Kuang, M. Duan, H. Chen, D. and Jiang, M., 2004. pH-dependent multiple morphologies of novel aggregates of carboxyl-terminated polymide in water. European Physical Journal E. Vol. 15 I. 2 p. 211-215.

Wang, J. Mei, J. Hu, R. Sun, J. Z. Qin, A. and Tang, B. Z., 2012. Click Synthesis, Aggregation-Induced Emission, E/Z Isomerization, Self-Organization, and Multiple Chromisms of Pure Stereoisomers of a Tetraphenylethene-Cored Luminogen. Journal of the American Chemical Society. Vol. 134 I. 24 p. 9956-9966.

Whitesides, G. and Grzybowski, B., 2002. Self-assembly at all scales. Science. Vol. 295 I. 5564 p. 2418-2421.

Yang, X. Grailer, J. J. Rowland, I. J. Javadi, A. Hurley, S. A. Steeber, D. A. and Gong, S., 2010a. Multifunctional SPIO/DOX-loaded wormlike polymer vesicles for cancer therapy and MR imaging. Biomaterials. Vol. 31 I. 34 p. 9065-9073.

Yang, Z. Wang, X. Yang, Y. Liao, Y. Wei, Y. and Xie, X., 2010b. Synthesis of Electroactive Tetraaniline-PEO-Tetraaniline Triblock Copolymer and Its Self-Assembled Vesicle with Acidity Response. Langmuir. Vol. 26 I. 12 p. 9386-9392.

Yao, W. Li, Y. Feng, C. Lu, G. and Huang, X., 2014. Synthesis of amphiphilic ABA triblock copolymer bearing PIB and perfluorocyclobutyl aryl ether-containing segments via sequential living carbocationic polymerization and ATRP. Polymer Chemistry. Vol. 5 I. 21 p. 6334-6343.

Yokoyama, M. Satoh, A. Sakurai, Y. Okano, T. Matsumura, Y. Kakizoe, T. and Kataoka, K., 1998. Incorporation of water-insoluble anticancer drug into polymeric micelles and control of their particle size. Journal of Controlled Release. Vol. 55 I. 2-3 p. 219-229.

Yu, Y. and Eisenberg, A., 1997. Control of morphology through polymer-solvent interactions in crew-cut aggregates of amphiphilic block copolymers. Journal of the American Chemical Society. Vol. 119 I. 35 p. 8383-8384.

Zeng, F. and Zimmerman, S., 1997. Dendrimers in supramolecular chemistry: From molecular recognition to self-assembly. Chemical reviews. Vol. 97 I. 5 p. 1681-1712.

Zhang, L. and Eisenberg, A., 1995. Multiple Morphologies of Crew-Cut Aggregates of Polystyrene-B-Poly(acrylic Acid) Block-Copolymers. Science. Vol. 268 I. 5218 p. 1728-1731.

Zhang, M. Xu, D. Yan, X. Chen, J. Dong, S. Zheng, B. and Huang, F., 2012. Self-Healing Supramolecular Gels Formed by Crown Ether Based Host-Guest Interactions. Angewandte Chemie-International Edition. Vol. 51 I. 28 p. 7011-7015.

Zhao, D. Neubauer, T. M. and Feringa, B. L., 2015a. Dynamic control of chirality in phosphine ligands for enantioselective catalysis. Nature Communications. Vol. 6 p. 6652-6652.

Zhao, Z. He, B. and Tang, B. Z., 2015b. Aggregation-induced emission of siloles. Chemical Science. Vol. 6 I. 10 p. 5347-5365.